Large-Area Ordered Superlattices from Magnetic Wüstite/Cobalt Ferrite Core/Shell Nanocrystals by Doctor Blade Casting

Maryna I. Bodnarchuk,[†,⊥,*] Maksym V. Kovalenko,[†,⊥] Stefan Pichler,[†] Gerhard Fritz-Popovski,[‡] Günter Hesser,[§] and Wolfgang Heiss[†,*]

[†]Institute of Semiconductor and Solid State Physics, University Linz, Altenbergerstrasse 69, 4040 Linz, Austria, [‡]Institute of Physical Chemistry, Karl-Franzens University, Heinrichstrasse 28, 8010 Graz, Austria, and [§]Center of Surface and Nanoanalytiks, University Linz, Altenbergerstrasse 69, 4040 Linz, Austria. [⊥]Present address: Department of Chemistry, The University of Chicago, Chicago, Illinois 60637.

ABSTRACT Although a large diversity of single-component and binary superlattices from colloidal nanocrystals have been demonstrated, applications of such ordered nanocrystal assemblies are still hampered due to a lack of control over the self-assembly processes over large areas. A reel-to-reel compatible large-area coating technique for solutions is given by doctor blade casting, which is applied here to deposit colloidal nanocrystals onto various substrates. The self-assembly process is demonstrated for magnetic nanocrystals, having a high potential for applications in magnetic memory devices. Shape-controlled (spherical and cubic) and monodisperse nanocrystals with a Wüstite core and a cobalt ferrite shell are used in particular. Doctor blade casting of these colloidal nanocrystals results in films exhibiting hexagonally closely packed arrangements, which are formed by a top-down growth, as is evidenced by cross sectional transmission electron microscopy. The ordering in the topmost layer extends over large areas, although some defects and irregularities are found. The degree and quality of self-assembly is quantified by analyzing plan view images of the assemblies by means of the decay of their autocorrelation function. This analysis reveals that the degree of ordering obtained by doctor blade casting outperforms those provided by alternative deposition techniques such as inkjet printing or drop casting. The results for the coherent lengths deduced from the autocorrelation analysis are shown to be consistent with those from grazing-incidence small-angle X-ray scattering, giving coherence length on the order of 1000 nm.

KEYWORDS: self-assembly · nanocrystals · ferrites · superlattices · doctor blade casting · autocorrelation

While first observations of two-dimensional ordering in clusters of micrometer-sized colloidal particles upon drying from solutions date back to the beginning of the 20th century,[1] in recent years, research on self-assembly focuses on particles which are up to 2 orders of magnitude smaller.[2] In particular, the self-assembly of colloidal nanocrystals (NCs) leads to a large diversity of single-component[3−17] and binary[18−27] superstructures with two- and three-dimensional ordering. Even though ordering represents a promising tool to create novel collective properties from NC assemblies (*e.g.*, due to modifications of their electronic states and the formation of minibands resulting from electronic coupling between individual NCs), applications of ordered NC assemblies in (opto-)electronic[7,8,12,18] or magnetic[9] devices have been hampered, due to the lack of efficient methods for the fabrication of well-ordered NC self-assemblies on large areas. On one hand, ordering might have a profound effect on the electronic transport in NC layers,[7,8] and on the other hand, it is evidently crucial for magnetic storage devices based on colloidal NCs,[9] not only to optimize their binary digit (bit) density but also to make individual NC bits reproducibly addressable for read/write events.

All known techniques for self-assembly of NCs take advantage of their solution processability and their naturally given tendency to form densely and ordered packing, driven by maximization of entropy[19] and eventually by specific interactions, such as dipole−dipole, van der Waals, and Coulomb interactions.[20,21] The used techniques to obtain ordered NC films on substrates include simple drop casting,[13] deposition by the Langmuir−Blodgett technique,[10,11] and by spin casting,[12] whereas by the latter, the pure colloidal solutions are not used but nanocrystal/conjugated polymer mixtures are, resulting in a phase separation during the deposition. In the present study, a reel-to-reel compatible large-area coating technique for solution-processable materials is applied for NC deposition, given by doctor blade casting (DBC), also known as tape casting.[28,29] The latter is the basic fabrication process in the important electronic

*Address correspondence to mbodnarchuk@uchicago.edu, wolfgang.heiss@jku.at.

Received for review September 24, 2009 and accepted December 15, 2009.

Published online December 22, 2009. 10.1021/nn901284f

ceramic industry, applied, for example, for deposition of multilayered capacitors and multilayered ceramic packages.[28] The DBC is applied in organic electronics also as a large-area coating process for printed bulk heterojunction solar cells[30] as well as for the fabrication of NC-sensitized organic photodiodes operating as organic/inorganic hybrid infrared imagers.[31] In this work, DBC is applied as a tool for large-area self-assembly of colloidal NCs into thin superlattice films with face-centered cubic (fcc) and hexagonal close-packed (hcp) structures. The lateral ordering of superlattices extends over large areas within micrometer-sized islands, while the vertical arrangement of layers suggests a top-down growth mechanism at the air−solvent interface.

The self-assembly process is demonstrated here for monodisperse magnetic heterostructured NCs, each consisting of a Wüstite (Fe_xO) core and a cobalt ferrite ($CoFe_2O_4$) shell,[32] further referred to as W/C NCs. Besides their interesting magnetic properties, such as exchange bias effects and vertical magnetization loop shifts,[32] they are chosen for this study mainly because of (i) their relatively large sizes in the range of 10−25 nm, (ii) their excellent colloidal stability and high tendency to self-assemble, and (iii) their convenient shape-controlled synthesis providing spherical and cubic NCs in the same size range. While (i) and (ii) make it very easy to observe fine details in the studied superlattices by scanning and transmission electron microscopy (SEM and TEM) performed on plan views and sample cross sections, (iii) allows the study of the effect of shape on NC self-assembly. At last, despite their relatively large sizes, each NC exhibits rather small magnetic moments due to the zero net magnetization of the antiferromagnetic Fe_xO cores, resulting in small energies for the dipolar interparticle interactions of less than 0.1 *kT*, which is minimizing the effect of magnetic dipolar interactions on the superlattice formation. The densely packed arrays of magnetic NCs are highly promising for magnetic data storage, assuming that each individual NC acts as a binary digit (bit) in a storage device.[9]

To quantify the degree and quality of the ordering, two statistical methods are applied here to analyze SEM and TEM images: (i) translational and orientational correlation functions, previously demonstrated for two-dimensional assemblies of colloidal particles,[33−35] and (ii) 2D autocorrelation functions (AF), which are routinely used for epitaxial quantum dot systems.[36,37] Both approaches are used to evaluate coherence lengths, and the results are compared with those measured by grazing-incidence small-angle X-ray diffraction (GISAX) experiments. We also compare the degree of ordering for DBC films with alternative deposition methods like drop casting or inkjet printing.

RESULTS AND DISCUSSION

Doctor Blade Casting of Ordered NC Films. To obtain thin and uniform NC films, DBC is performed on freshly hydrophobized Si substrates or on Si substrates covered with a 100 nm layer of platinum. For a systematic study of NC self-assembly, a substrate size of 1 × 1 in.^{2} was used in all experiments, even though much larger substrates were exemplarily tested to give equivalent results as those obtained for the small ones. The DBC is schematically shown in Figure 1A. The films are formed by dropping 30−50 μL of NC colloid on one end of the substrate and subsequently moving the blade over the substrate with constant speed to uniformly spread the colloid over the whole sample area. The gap between the blade and the surface was adjusted to 2 mm for all experiments, and the substrates were kept at a temperature of 60 °C (for chlorobenzene as a solvent), resulting in a complete drying of solvent within 5−10 s. After film deposition, the excess of the colloidal solution was re-collected from the blade edge for further use, making the DBC process very material efficient. The initial experiment was performed with a colloidal solution containing monodisperse W/C NCs with spherical shape and a diameter of 11 nm (Figure 1B) with a standard size deviation of ±4.5% (inset in Figure 1C). These NCs are stabilized with an oleate ligand shell, and the addition of a small excess of oleic acid to the colloidal solution assists the self-assembly into ordered superstructures, as has been previously observed by others.[14,20]

A first inspection of the deposited NCs by optical microscopy shows a smooth and uniform film all over the substrate. A closer inspection shows that the surface is completely covered with tightly closed islands (Figure 1C). Only close to the substrate edges are the islands thicker and often separated from each other. Unlike drop casting, no lateral shrinking of solution or significant accumulations of NCs at the contact line of the liquid[38] are observed. The absence of any surface patterns of NC precipitates within the films, which are frequently observed upon NC deposition from droplets and arise from gradients in surface tension resulting from gradients in temperature and concentration,[39] suggests that by the DBC also these so-called Marangoni flows[40] are greatly suppressed. SEM images reveal in addition the self-assembly of the NCs in detail (Supporting Information Figure S1), especially when the images are "flattened" with respect to background brightness variations caused by fluctuations in film thickness (Figure 1D). Such flattened images highlight the ordering of the NCs; they show defects in the two-dimensional superstructures, and they allow the evaluation of AF correlation lengths, providing a convenient measure to compare the quality obtained by different colloids and different deposition techniques. By DBC, we obtained thin film superlattices from differently

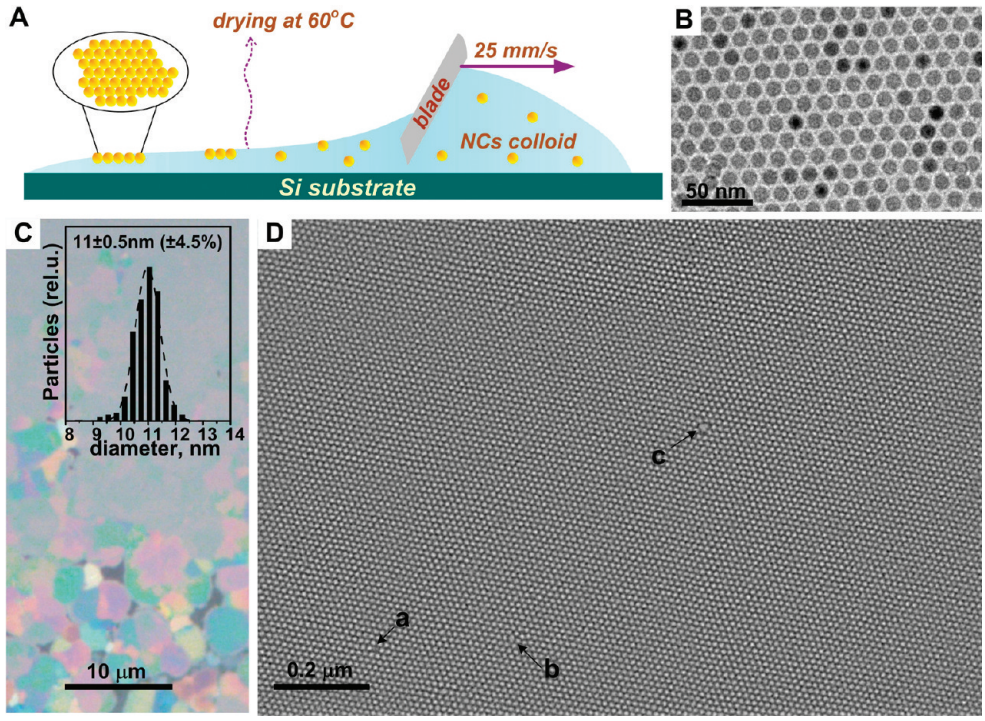

Figure 1. (A) Sketch of the DBC process where the NCs assemble at the liquid/air interface. (B) TEM image of the used W/C NCs with a size of 11 nm. (C) Optical microscope image of the NC film exhibiting separate islands only at the boarder of the substrate. The inset shows the size distribution of the 11 nm W/C NCs used. (D) Background flattened SEM image of the 11 nm W/C NCs deposited by DBC on a Pt-covered Si substrate. The labeled arrows indicate point defects in the NC superlattice.

sized and shaped NCs dispersed in various nonpolar solvents (Table 1).

Island Formation and Top-Down Growth in NC Multilayers. The details of NC film formation are studied by electron microscopy. Since the brightness in SEM images is related to the electron interaction volume, multilayers of NCs appear brighter as more layers contribute to the electron scattering. Thus, the darkest regions in the plan view image in Figure 2A represent the substrate, visible due to cracks in the NC assemblies, which are most probably formed during late stages of solvent drying, because the resulting islands fit to each other like pieces of a puzzle. The areas covered by the NCs appear significantly brighter as the substrate, and within these areas, step-like fluctuations in brightness are observed, depending on the number of NC monolayers (MLs) interacting with the electron beam (the brightest spots in Figure 2A are caused by local charging). By increasing the magnification, the areas covered by 1 to 3 ML can be clearly distinguished (Figure 2B) and the ordering of the NCs is observed. Using the same colloid, similar assembled patterns are found by transmission electron microscope (TEM) imaging for thin superlattices deposited on a carbon-coated TEM grid by drying from a droplet (Figure 2C). Also, by TEM, thickness variations of the film between one and several MLs are observed. In particular, at least one NC ML covers the complete area shown in Figure 2C, whereas fractions of a second and a third ML stacked on each other are also observed. The hexagonal arrangement of NCs seen in the SEM and TEM images of the single ML suggests either a face-centered cubic (fcc) or a hexagonal close- packed (hcp) lattice of the NC superstructures. Starting from a coverage corresponding to 3 MLs, the difference between these two crystal structures becomes apparent. Both appear as hexagonally arranged when they are viewed along their [111] axis (for the fcc lattice) and their [001] axis (for the hcp lattice). In the [001] direction, the hcp

TABLE 1. List of Investigated Samples Prepared from Colloidal W/C NCs of Different Size and Shape[a]

sample	shape	size/nm	solvent	substrate	deposition	$\xi_{0.5}$ [nm]	NCs
W/C1−S1	spheres	11	CB	Pt	DBC	303 ± 5	22
W/C1−S2	spheres	11	CB	Si	DBC	380 ± 5	25
W/C2−S3	spheres	20	CB	Si	DBC	220 ± 25	10
W/C2−S4	spheres	20	CF	Si	DBC	106 ± 5	5
W/C3−S5	spheres	11	CB	Si	inkjet	96 ± 5	6
W/C4−S6	cubes	11	CB	Si	DBC		

[a]Given is also the used solvent (CB, chlorobenzene; CF, chloroform), the substrate, the deposition technique, and the evaluated correlation length $\xi_{0.5}$ corresponding to a certain number of NCs.

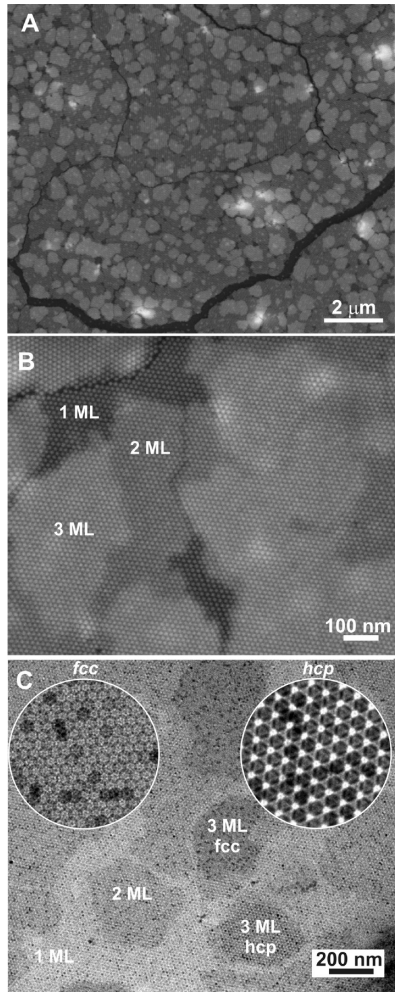

Figure 2. (A) Low-resolution and (B) high-resolution SEM images of an ordered NC film prepared by DBC of 11 nm W/C NCs from a chlorobenzene solution. (C) Low-resolution TEM images of NC superlattices prepared by drop casting using the same solution as was used for (A) and (B). The insets illustrate the difference between the (111) projection of fcc and the (001) projection of hcp lattices.

structure is a repeated sequence of two hexagonally ordered layers and it exhibits holes through the entire structure (right inset in Figure 2C). In the fcc lattice, composed of periodic stacking of three layers in the [111] direction, these holes are absent (left inset in Figure 2C). Indeed, we observe both structures with similar occurrence by TEM imaging.

To get further insights into the superlattice formation by DBC, we cut thin slices from the samples by focused ion beam (FIB) and examined them by cross sectional TEM imaging. To protect the NC assemblies during the FIB preparation of thin lamellas, the superlattice films deposited onto Si substrates were first capped by a thermally evaporated 200 nm SiO_2 layer. The cross sectional TEM images show that the topmost NC ML shows the largest lateral expansion, while the subjacent second and third layers show much smaller lateral extends. This observation suggests that the NC assemblies exhibit a "top-down" growth, starting from the

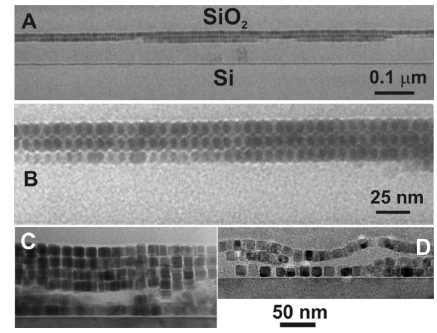

Figure 3. Cross sectional TEM images of a thin NC superlattice formed at the top interface by (A,B) 11 nm spherical and 11 nm cubic $Fe_xO/CoFe_2O_4$ NCs (C,D).

liquid−air interface and proceeding toward the substrate (as sketched in Figure 1A). This top-down growth also clarifies why the ordering of NCs shown in Figure 2B is limited by the cracks but is not affected by the boundaries of the individual islands with 2 or 3 NC layer coverage. The second and third NC layers apparently nucleate when the first layer is already formed. Even though the top-down growth is somewhat counterintuitive, our observation is in agreement with several reports in literature. Recently Friedrich *et al.*[24] reported a top-down assembly in binary NC superlattices, investigated by TEM tomography. A similar growth mechanism in binary NC superlattices has been recently suggested also by Korgel *et al.*[41] Furthermore, our investigation is in full agreement with the results of Bigioni *et al.*,[14] who studied the formation of ordered dodecanethiol-capped Au NCs and proposed a model explaining this observation by an evaporation-induced kinetic trapping of the NCs at the liquid−air interface. The latter is favored if the diffusion of the NCs within the solvent is slower as the evaporation rate of the solvent. In our case, this condition is fulfilled because the evaporation of the approximately 50 μm thick liquid layer of chlorobenzene takes approximately 5 s at the chosen substrate temperature of 60 °C, whereas during this evaporation time, the spherical 11 nm large W/C NCs with a hydrodynamic radius of ~7.5 nm (taking into account the ~2 nm oleate shell) diffuse a vertical distance of about 25 μm (this diffusion length is estimated from Stokes−Einstein relation taking into account the viscosity of chlorobenzene at 60°C ($\eta = 0.5$ mPa · s)).[42] According to the model, the self-assembly depends also on the change of the surface tension $\Delta\sigma$ caused by the adsorption of one NC and thus it should exhibit a strong solvent dependence. Such a strong solvent dependence we indeed observe, as will be described further below. Figure 3 reveals also that the NC layers are lifted above the Si substrate surface. This observation we attribute to the presence of an underlying layer of excessive stabilizer, required to obtain a long-range ordering in the films. Also the pinning of the NC film by NC aggregates can play a role.

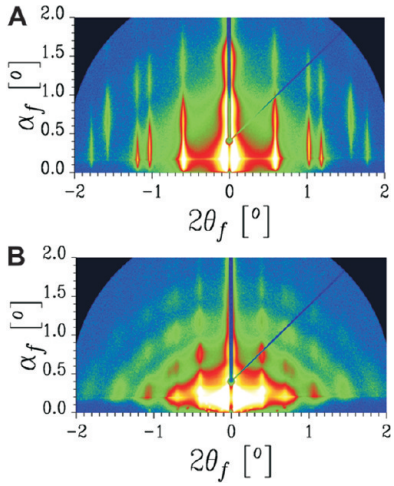

Figure 4. GISAXS patterns for a thin superlattice of (A) 11 nm and (B) 20 nm $Fe_xO/CoFe_2O_4$ NCs prepared by doctor blade casting from the colloidal solution.

Ordering Observed by X-ray Diffraction Experiments. Besides the direct evaluation of microscopy images, a standard method to estimate crystal structure and to quantify degree of ordering in thin films is given by grazing-incidence small-angle X-ray scattering (GISAXS) experiments.[5,15,41] The GISAXS experiments were performed for the spherical W/C NCs with a size of 11 and 20 nm, deposited on hydrophobized Si substrates. The GISAXS pattern shown in Figure 4A is collected from a surface area of 0.48 mm^2. The sharp vertical stripes indicate a large degree of ordering. Their distances in the $2\theta_f$ direction follow the pattern of 11/2:31/2:41/2:71/2:91/2, which is characteristic for a hexagonal arrangement of the NCs, with a lattice parameter of 15.9 nm. The peak width corresponds to correlations on the order of 1000 nm. The shape of the peaks in vertical direction can be attributed at small angles to a Yoneda peak[43] with $\alpha_c = 0.2°$, which corresponds to the critical angle of the silicon substrate. The minima in intensity at larger angles are due to the form factor of the particles, and they are well-described by scattering from homogeneous spheres with a diameter of 11.5 nm. For comparison, the GISAXS image of a film prepared from the 20 nm large W/C NCs shows basically the same arrangement (Figure 4B). The hexagonal lattice shows correlations up to 250 nm, which is considerably less than what is obtained in the case of the 11 nm NCs. The vertical intensity pattern of the stripes can be explained by spheres of 19.5 nm in diameter and some surface roughness, which leads to a stronger decay of intensity.

Quantification of Ordering in the Topmost NC Layer. While the GISAXS is sensitive to the ordering of NCs located directly at the surface as well as to that of buried NCs, the top-down growth implies that the highest degree of order is obtained on the topmost NC layer. Thus, we go back now to the evaluation of the ordering by analyzing the SEM images, which are "background flattened" in such a way that exclusively the NCs of the topmost ML become apparent. As described above, the ordering is, on one hand, limited by the cracks in the film, acting as boundaries for the ordered areas within the film. Inspecting the SEM image of the 11 nm W/C NC assembly shown in Figure 1D makes evident that the ordering is not solely limited by these domain boundaries but also by some other defects in the NC lattice, such as vacancies (labeled "a" in Figure 1D) or the incorporation of NCs with a nonfitting size (labeled "b" and "c"). To obtain an accurate statistical measure for the degree of ordering present in NC assemblies, usually the translational or pair correlation function $g(r)$ and the orientational distribution function $g_6(r)$ are employed[33−35,44] (a detailed evaluation of these two

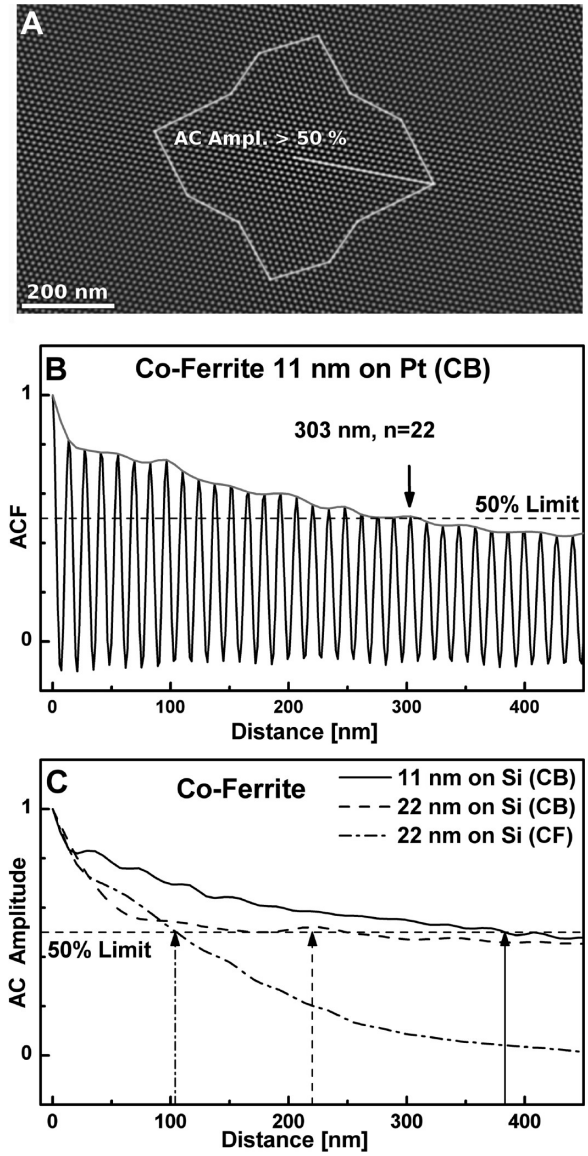

Figure 5. Two-dimensional AF from the image shown in Figure 1C. The straight white line indicates the Γ-M direction within the hexagonal lattice for which the profile of the AF is shown in (B). Within the indicated area in (A), the amplitude of the AF exceeds 50%. The envelope of the AF in (B) reaches the 50% limit at a distance of 303 nm. (C) Envelops of AFs obtained for various NC sizes, solvents, substrates, and deposition techniques (see labels).

functions for the ordered NC system shown in Figure 1D is given in the Supporting Information). The $g(r)$ and $g_6(r)$ are oscillating functions (Supporting Information Figure S2), and the decay of their oscillation amplitude as function of the distance r allows one to classify the kind of ordering[35] as well as to determine a correlation length ξ. In our case, both functions confirm the presence of a true long-range ordered system, the quantification of a coherence length (*e.g.*, from a fit of $g(r)$ with a Ornstein−Zernike behavior [$g_{OZ}(r) \sim \exp(-r/\xi)/r)$][45]) is however difficult because, for the present NC assembly, the envelope function of $g(r)$ matches so closely to $1/r$ that $g_{OZ}(r)$ becomes very insensitive to ξ. Thus, here we suggest another method to quantify the ordering in NC films, which has been frequently applied to self-assembled epitaxial quantum dot systems. Instead of numerically calculating the ordering parameters $g(r)$ and $g_6(r)$, simply the two-dimensional autocorrelation function (2d-AF) of the image can be used to define a measure for the degree of ordering.[36,37] The AF has additional advantages that it is (i) conveniently obtained by applying a freely available data visualization and analysis software (Gwyddion) and (ii) sensitive not only to NC positions but also to variations of the NC size and shape. The 2d-AF from the assembly of the 11 nm sized W/C NCs shown in Figure 1D is periodic, and its maxima again show a hexagonal lattice (Figure 5A). More quantitative information can be deduced from the profile of the AF, taken from the center of the image (Γ) along one of the main axis of the hcp lattice (Γ-K, indicated by a white line in Figure 5A). This line profile, shown in Figure 5B, exhibits oscillations due to correlations and anticorrelations, and its envelope decays with increasing distance from the Γ point at $r = 0$. Irrespective of the shape of this decay, we define a correlation length $\xi_{0.5}$ at the distance where the AF drops to 50% (indicated by the dashed line in Figure 5B,C). For the doctor bladed 11 nm NC film on Pt-covered substrate, we find $\xi_{0.5} = 303$ nm, within this distance $n = 22$ NCs are perfectly aligned along the Γ-K direction of the lattice (Figure 5B and W/C1−S1 in Table 1). Since the $\xi_{0.5}$ limit exhibits also a small directional dependence, for a systematic comparison between different samples, the correlation lengths are always taken for the crystal axes giving the highest value for $\xi_{0.5}$. It should be noted also that the evaluated correlation length is clearly smaller than the size of the evaluated image and is also smaller than the size of the ordered domains shown in Figure 2, thus indeed the number of defects in the lattice is limiting the correlation lengths.

Comparison between Various NC Colloids and Deposition Techniques. ***Comparison with Epitaxially Grown Quantum Dots.*** To judge how excellent the degree of ordering in the films, prepared by DBC, can be, $\xi_{0.5}$ is evaluated for various different ordered NC systems. First of all, the ordering of the NCs demonstrated above by DBC is by far better than what was obtained so far in any epitaxial quantum dot system. The AF of two-dimensional ordered (In,Ga)As quantum dots, grown by molecular beam epitaxy, for example, usually shows only a few (<10) oscillations and its envelope decays so rapidly that $\xi_{0.5}$ only reaches up to the nearest neighbor quantum dots.[36] The situation is better in epitaxial quantum dot superlattices from IV−VI materials for which, in the best cases, $\xi_{0.5}$ values are found corresponding to $n = 6$ quantum dots aligned into one direction.[37]

Size Effect on NC Ordering. While the self-assembly was demonstrated above for 11 nm NCs, also larger W/C NCs exhibit a hcp ordering when they are deposited by DBC (Supporting Information Figure S3); however, for 20 nm NCs in size, the obtained correlation length is reduced to 220 nm (W/C2−S3 in Table 1 and Figure 5C). Size effects from the self-assembly process are also expected according the model considerations from Bigioni *et al.*:[14] If the NC size is too small, the gain of the surface energy provided by the NCs impinging on the liquid−air interface during top-down growth $\Delta\sigma$ can not compensate the thermal energy, and the NCs are immediately displaced from the liquid−air interface.[46] As a result, no ordering is obtained. On the opposite, if the NC size is too large, interparticle forces can cause the NCs to localize on the bottom of the first layer rather than at the top interface, preventing any large-area assembly. This can also cause the NCs to assemble into large pieces rather than into thin superlattice film. This effect we indeed observed by the cross sectional TEM images of the 20 nm large W/C NCs (Figure S4).

Solvent and Stabilizer Effect. By making use of the same NCs, 20 nm size, but by changing the solvent from chlorobenzene to chloroform, a further decrease of the correlation length to 106 nm is observed (Figure 5C and WC2−S4 in Table 1). No ordered domains were formed when hexane was used as solvent.[5] The reason for this strong solvent dependence is attributed to the differences in surface tension. Hexane has a considerably lower surface tension (18 mN/m) compared to chlorobenzene (33 mN/m). This observation is in agreement with the finding that addition of ethanol ($\sigma = 22$ mN/m) to chlorobenzene also leads to a complete inhibition of ordering during the self-assembly process. Another important factor is the concentration of stabilizer excess: The best ordering is obtained for the highest concentration of stabilizer added, which was roughly equal to the amount of NCs. For highly purified NC colloids, in contrast, no self-assembly was observed. The important role of a stabilizer excess was already observed by several other groups, reporting long-range ordered single-component[14,16] as well as binary superlattices.[19,20,25,41] There are several effects which can be associated with the presence of excessive stabilizer molecules such as oleic acid. First, oleic acid can alter the surface tension at the liquid−air interface. Second, as a low volatile substance, oleic acid can reduce the evaporation rate at the late stages of drying, which

was postulated to be favorable for NC assembly in the case of CdSe−Au binary superlattices and dodecanethiol as excessive ligand.[26] Third, it can alter the interparticle interaction due to the so-called depletion interaction.[41]

DBC versus Other Deposition Techniques. Besides the NC size, the choice of solvent, the substrate, and the excess of stabilizer, the deposition technique itself is important to obtain long-range ordered NC films. Highly ordered NC arrays were presented by Lin *et al.*,[13] who investigated drop casting of colloidal suspensions containing dodecanethiol-covered Au NCs. Using published SEM images of these highly ordered Au NCs and applying the AF analysis, we obtained $\xi_{0.5} = 220$ nm, which is smaller than what we have obtained for the 11 nm W/C NCs. For the latter, an improved ordering is obtained when they are cast on hydrophobic Si surfaces. In this case, the decay of the AC envelope reaches the 50% limit at a length of 380 nm (Figure 5C and W/C1−S2 in Table 1), which is the best value we obtained.

An alternative to the DBC to obtain homogeneous NC films on large scales could be inkjet printing, which was demonstrated to be a well-controlled deposition technique for NCs.[47,48] For the inkjet printing of W/C NCs, where basically the same processes used for drop casting, such as the accumulation of NCs at boarder lines due to the coffee-stain effect, are relevant,[47] we observe ordering. In this case, however, only 6 periods of the AF are found within the 50% limit (W/C3−S5 in Table 1), while by the DBC, much longer correlation lengths were obtained.

DBC of Cubic NCs. Self-assembly of NCs is not necessarily restricted to spherical species, but it has been applied to shapes such as nanorods,[49] hexagons,[50] or cubes.[17,50−52] For cubes, however, the self-assembly is much more sensitively dependent on size homogeneity than those of closed-packed nanospheres or hexagons[50] because of the higher space-filling factors in nanocube lattices. Thus, as a final proof to demonstrate the suitability of DBC to obtain ordered NC assemblies, we applied it to NCs with cubical shape. Recently, Ahniyaz *et al.*[17] demonstrated a way to achieve ordered maghemite nanocube arrangements. By drop casting dilute toluene-based dispersions, mosaics such as nanocube arrays were obtained, and long-range ordering was achieved by applying an external magnetic field during the initial stage of the assembly process.[17]

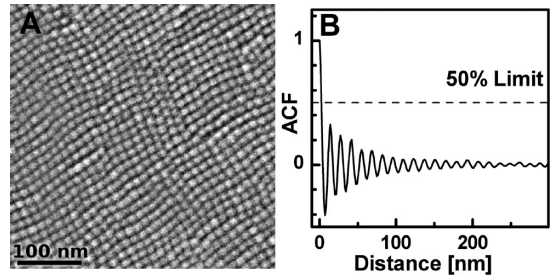

Figure 6. (A) Self-assembly of W/C NCs with cubic shape, deposited by DBC on a Si substrate. (B) AF-profile of the image in (A) exhibits oscillations; however, all of them are below the 50% limit.

By DBC of cubic-shaped W/C NCs on hydrophobized Si substrates, however, we obtained ordering, even without any magnetic field. In this case, all nanocubes become oriented with their [100] facets parallel to the sample surface. As shown in Figure 6, the degree of ordering is not as good as that obtained for the spherical NCs, although the cubes exhibit nearly the same excellent size dispersion as the spheres. Anyway, the AF in Figure 6B exhibits oscillations up to several 100 nm, while in the literature, so far, self-assembly of $CoFe_2O_4$ nanocubes has been demonstrated only over shorter length scales.[50−52]

CONCLUSION

The homogeneous deposition of NC colloids by DBC is shown to result in a top-down growth of ordered NC assemblies. The ordering emerges during the drying of the solvent at the liquid/air interface, and it depends on parameters such as the NC size, choice of solvent, excess of stabilizer, wetting property of the substrate, and shape of the NCs. Besides GISAXS experiments, as a measure for the quality of ordering, the decay of the AF of the SEM images is used to obtain a correlation length. The latter reaches values of up to 380 nm for optimized deposition conditions and an optimal choice of NCs, given by monodisperse W/C core−shell NCs with spherical shape and a size of 11 nm. This correlation length is larger than what can be deduced from ordered assemblies given in literature, and it is related to defects in the NC lattices rather than to the domain size of the ordered areas being much larger than the correlation length. All of these findings evidence the appropriateness of DBC as a prime technology to obtain large-area ordering from colloidal NCs in single-component superlattices.

METHODS

W/C NC Synthesis. $Fe_xO/CoFe_2O_4$ core−shell NCs capped with oleic acid molecules were prepared by solution-phase colloidal synthesis based on a thermal decomposition of mixtures of metal oleates in high-boiling organic solvents. The details of the synthesis and purification can be found in ref 32. Spherical 11 nm NCs were grown at 305 °C in a octadecene/phenyl ether mixture (1:1 v/v) in the presence of oleic acid as stabilizer, whereas 11 nm cubic NCs were prepared at 320 °C by adding sodium oleate as shape-regulating ligand. For the 20 nm large spherical NCs, the growth temperature was raised to 320 °C.

Growth of NC Superlattices by DBC. Well-purified W/C NCs were dissolved in chlorobenzene at a concentration of $\sim 10^{14}$ cm^{-3}. Oleic acid was added to this solution up to a concentration of 1−2 μg cm^{-3}. Colloidal solutions of W/C NCs were cast onto the Si (or Pt-coated Si) substrates using a commercial coater from Erichsen GmbH (Coatmaster 509/MC-I). This equipment consists of a

heated glass plate on which the substrates can be fixed and a motorized translation stage, moving a scraping blade with constant speed across the substrate. The blade speed can be varied, and the distance between blade and substrate surface is adjusted by a micrometer screw. The relatively fast movement of the blade across the substrate causes a uniform spreading of the colloidal solution which is dropped close to one sample edge. The spread of the droplet to a thin homogeneous liquid layer prevents any shrinkage of the wetted area during drying, such as would be observed during drying of a solvent droplet deposited on a flat substrate. Before deposition, the used Si substrates were freshly hydrophobized by dipping into HF or by a standard treatment with hexamethyldisilane. The one square inch Si substrates were fixed on the coater hot plate kept at 60 °C; 30−50 μL of NC colloid was placed close to one end of the substrate, and the liquid was cast over the entire substrate by the moving blade. The gap between the blade and the substrate surface was adjusted to 2 mm, and the blade velocity was set to 5−25 mm s^{-1} to control the thickness of the resulting NC film.

Structural Characterization of NC Superlattices. To prepare slices for cross sectional TEM imaging, the NC films on Si substrates were protected by a 100 nm thick layer of thermally evaporated SiO_2. All further preparation was performed with a Zeiss CrossBeam 1540 scanning electron microscope (SEM), which is equipped with the focused ion beam (FIB) column, including a gas inlet system and a micromanipulator. A further protection layer (tungsten) was deposited using the FIB with Ga ions and a decomposable W source. Subsequently, a 100 nm thin, 20 μm long, and 5 μm deep slice was cut from the sample by the FIB, and the slice was transferred onto a copper TEM grid. The final thinning of the specimen to about 100 nm is performed by slow FIB etching, and it is monitored by the SEM. The TEM images were acquired using a FasTEM 2011 electron microscope (JEOL) operating at 200 keV accelerating voltage.

Grazing-Incidence Small-Angle X-ray Scattering. Same samples as for SEM and TEM studies were used for the grazing-incidence small-angle X-ray scattering (GISAXS) experiments. These experiments were conducted at the beamline BW4 of the HASYLAB/DESY synchrotron facility using the microbeam setup.[53,54] The wavelength used was 0.1381 nm, and the primary beam had a focal spot size of 17 × 60 μm^2. Using an incidence angle of 0.4°, this resulted in a footprint on the sample of 0.071 × 8.6 mm^2. The primary beam and the reflected beam were blocked by two beam stops. The scattering intensity was recorded using a two-dimensional CCD detector (MarResearch) at a sample to detector distance of 2249 mm. The CCD had a resolution of 2048 × 2048 pixels with a pixel size of 79.1 μm. GISAXS data were evaluated using the program IsGISAXS[49] using the framework of the distorted wave Born approximation.[55,56]

Processing of AF Images. To correctly perform an autocorrelation analysis of the topmost layer of the NC film, the non-uniform background in the SEM images arising from variations in thickness due to any underlying materials (isolated NC islands or accumulated excess of stabilizer) have to be removed. These darkened areas have to be removed without affecting any information concerning the NC ordering within the uppermost layer. To obtain this background flattening, we made use of the GNU image manipulation tool (GIMP) to perform a Gaussian blurring of the whole image, with a blur radius in the order of several NC radii. The image created by the blurring contains exclusively the long-range gray scale modulations due to the fluctuating thickness of the film. This image from the background was then subtracted from the original SEM image, leaving the information provided by the topmost NC layer. For such "background flattened" images, the AF was generated by making use of the "Gwyddion" scanning probe microscopy analyzing software. The 2d-AF cross-correlates the image with itself, revealing its self-similarity as function of displacement. Line scans from the 2d-AF represent the one-dimensional AF in a particular direction.

Acknowledgment. This work has been supported by the Austrian Nano-Initiative (project NSI) and by the Austrian Science Found FWF (project START Y179). G.F.P. wants to thank HASYLAB at DESY for beamtime and S. V. Roth and A. Timmann for support during the GISAXS experiments.

Supporting Information Available: Evaluation of the correlation functions $g(r)$ and $g_6(r)$ of the nanocrystal assemblies is described and their results are shown in Figure S2. The original SEM images of the background flattened image in Figure 1D is given in Figure S1. Furthermore, plan view and cross sectional images of self-assemblies obtained with 20 nm large nanocrystals are shown. This material is available free of charge *via* the Internet at http://pubs.acs.org.

REFERENCES AND NOTES

1. Perrin, J. Brownian Motion and Molecular Reality. *Ann. Chim. Phys.* **1909**, *18*, 5–114.
2. Whitesides, G. M.; Grzybowski, B. Self-Assembly at All Scales. *Science* **2002**, *295*, 2418–2421.
3. Fried, T.; Shemer, G.; Markovich, G. Ordered Two-Dimensional Arrays of Ferrite Nanoparticles. *Adv. Mater.* **2001**, *13*, 1158–1161.
4. Sun, S. H.; Murray, C. B. Synthesis of Monodisperse Cobalt Nanocrystals and Their Assembly into Magnetic Superlattices. *J. Appl. Phys.* **1999**, *85*, 4325–4330.
5. Urban, J. J.; Talapin, D. V.; Shevchenko, E. V.; Murray, C. B. Self-Assembly of PbTe Quantum Dots into Nanocrystal Superlattices and Glassy Films. *J. Am. Chem. Soc.* **2006**, *128*, 3248–3255.
6. Yin, M.; Chen, Z. Y.; Deegan, B.; O'Brien, S. Wustite Nanocrystals: Synthesis, Structure and Superlattice Formation. *J. Mater. Res.* **2007**, *22*, 1987–1995.
7. Talapin, D. V.; Murray, C. B. PbSe Nanocrystal Solids for n- and p-Channel Thin Film Field-Effect Fransistors. *Science* **2005**, *310*, 86–89.
8. Kovalenko, M. V.; Scheele, M.; Talapin, D. V. Colloidal Nanocrystals with Molecular Metal Chalcogenide Surface Ligands. *Science* **2009**, *324*, 1417–1420.
9. Sun, S.; Murray, C. B.; Weller, D.; Folks, L.; Moser, A. Monodisperse FePt Nanoparticles and Ferromagnetic FePt Nanocrystal Superlattices. *Science* **2000**, *287*, 1989–1992.
10. Collier, C. P.; Saykally, R. J.; Shiang, J. J.; Henrichs, S. E.; Heath, J. R. Reversible Tuning of Silver Quantum Dot Monolayers through the Metal-Insulator Transition. *Science* **1997**, *277*, 1978–1981.
11. Aleksandrovic, V.; Greshnykh, D.; Randjelovic, I.; Frömsdorf, A.; Kornowski, A.; Roth, S. V.; Klinke, C.; Weller, H. Preparation and Electrical Properties of Cobalt-Platinum Nanoparticle Monolayers Deposited by the Langmuir−Blodgett Technique. *ACS Nano* **2008**, *2*, 1123–1130.
12. Coe-Sullivan, S.; Steckel, J. S.; Woo, W. K.; Bawendi, M. G.; Bulovic, V. Large-Area Ordered Quantum-Dot Monolayers *via* Phase Separation During Spin-Casting. *Adv. Funct. Mater.* **2005**, *15*, 1117–1124.
13. Lin, X. M.; Jaeger, H. M.; Sorensen, C. M.; Klabunde, K. J. Formation of Long-Range-Ordered Nanocrystal Superlattices on Silicon Nitride Substrates. *J. Phys. Chem. B* **2001**, *105*, 3353–3357.
14. Bigioni, T. P.; Lin, X. M.; Nguyen, T. T.; Corwin, E. I.; Witten, T. A.; Jaeger, H. M. Kinetically Driven Self Assembly of Highly Ordered Nanoparticle Monolayers. *Nat. Mater.* **2006**, *5*, 265–270.
15. Connolly, S.; Fullam, S.; Korgel, B.; Fitzmaurice, D. Time-Resolved Small-Angle X-ray Scattering Studies of Nanocrystal Superlattice Self-Assembly. *J. Am. Chem. Soc.* **1998**, *120*, 2969–2970.
16. Park, J.; Kang, E.; Son, S. U.; Park, H. M.; Lee, M. K.; Kim, J.; Kim, K. W.; Noh, H. J.; Park, J. H.; Bae, C. J.; Park, J. G.; Hyeon, T. Monodisperse Nanoparticles of Ni and NiO: Synthesis, Characterization, Self-Assembled Superlattices, and Catalytic Applications in the Suzuki Coupling Reaction. *Adv. Mater.* **2005**, *17*, 429–434.
17. Ahniyaz, A.; Sakamoto, Y.; Bergstrom, L. Magnetic Field-Induced Assembly of Oriented Superlattices from Maghemite Nanocubes. *Proc. Natl. Acad. Sci. U.S.A.* **2007**, *104*, 17570–17574.

18. Urban, J. J.; Talapin, D. V.; Shevchenko, E. V.; Kagan, C. R.; Murray, C. B. Synergism in Binary Nanocrystal Superlattices Leads to Enhanced p-Type Conductivity in Self-Assembled PbTe/Ag_2Te Thin Films. *Nat. Mater.* **2007**, *6*, 115–121.
19. Chen, Z.; O'Brien, S. Structure Direction of II−VI Semiconductor Quantum Dot Binary Nanoparticle Superlattices by Tuning Radius Ratio. *ACS Nano* **2008**, *2*, 1219–1229.
20. Shevchenko, E. V.; Talapin, D. V.; Kotov, N. A.; O'Brien, S.; Murray, C. B. Structural Diversity in Binary Nanoparticle Superlattices. *Nature* **2006**, *439*, 55–59.
21. Kalsin, A. M.; Fialkowski, M.; Paszewski, M.; Smoukov, S. K.; Bishop, K. J. M.; Grzybowski, B. A. Electrostatic Self-Assembly of Binary Nanoparticle Crystals with a Diamond-like Lattice. *Science* **2006**, *312*, 420–424.
22. Overgaag, K.; Evers, W.; de Nijs, B.; Koole, R.; Meeldijk, J.; Vanmaekelbergh, D. Binary Superlattices of PbSe and CdSe Nanocrystals. *J. Am. Chem. Soc.* **2008**, *130*, 7833–7835.
23. Redl, F. X.; Cho, K. S.; Murray, C. B.; O'Brien, S. Three-Dimensional Binary Superlattices of Magnetic Nanocrystals and Semiconductor Quantum Dots. *Nature* **2003**, *423*, 968–971.
24. Friedrich, H.; Gommes, C. J.; Overgaag, K.; Meeldijk, J. D.; Evers, W. H.; de Nijs, B.; Boneschanscher, M. P.; de Jongh, P. E.; Verkleij, A. J.; de Jong, K. P.; van Blaaderen, A.; Vanmaekelbergh, D. Quantitative Structural Analysis of Binary Nanocrystal Superlattices by Electron Tomography. *Nano Lett.* **2009**, *9*, 2719–2724.
25. Chen, Z.; Moore, J.; Radtke, G.; Sirringhaus, H.; O'Brien, S. Binary Nanoparticle Superlattices in the Semiconductor−Semiconductor System: CdTe and CdSe. *J. Am. Chem. Soc.* **2007**, *129*, 15702–15709.
26. Lu, C.; Chen, Z.; O'Brien, S. Optimized Conditions for the Self-Organization of CdSe−Au and CdSe−CdSe Binary Nanoparticle Superlattices. *Chem. Mater.* **2008**, *20*, 3594–3600.
27. Shevchenko, E. V.; Ringler, M.; Schwemer, A.; Talapin, D. V.; Klar, T. A.; Rogach, A. L.; Feldmann, J.; Alivisatos, A. P. Self-Assembled Binary Superlattices of CdSe and Au Nanocrystals and Their Fluorescence Properties. *J. Am. Chem. Soc.* **2008**, *130*, 3274–3275.
28. Mistler, R. E. Tape Casting—The Basic Process for Meeting the Needs of the Electronics Industry. *Am. Ceram. Soc. Bull.* **1990**, *69*, 1022–1026.
29. Hotza, D.; Greil, P. Aqueous Tape Casting of Ceramic Powders. *Mater. Sci. Eng. A* **1995**, *202*, 206–217.
30. Schilinsky, P.; Waldauf, C.; Brabec, C. J. Performance Analysis of Printed Bulk Heterojunction Solar Cells. *Adv. Funct. Mater.* **2006**, *16*, 1669–1672.
31. Rauch, T.; Boberl, M.; Tedde, S. F.; Furst, J.; Kovalenko, M. V.; Hesser, G. N.; Lemmer, U.; Heiss, W.; Hayden, O. Near-Infrared Imaging with Quantum-Dot-Sensitized Organic Photodiodes. *Nat. Photonics* **2009**, *3*, 332–336.
32. Bodnarchuk, M. I.; Kovalenko, M. V.; Groiss, H.; Resel, R.; Reissner, M.; Hesser, G.; Lechner, R. T.; Steiner, W.; F., S.; Heiss, W. Exchange-Coupled Bimagnetic Wüstite/Metal Ferrite Core/Shell Nanocrystals: Size, Shape, and Compositional Control. *Small* **2009**, *5*, 2247–2252.
33. Ramos, L.; Lubensky, T. C.; Dan, N.; Nelson, P.; Weitz, D. A. Surfactant-Mediated Two-Dimensional Crystallization of Colloidal Crystals. *Science* **1999**, *286*, 2325–2328.
34. Terao, T.; Nakayama, T. Crystallization in Quasi-Two-Dimensional Colloidal Systems at an Air−Water Interface. *Phys. Rev. E* **1999**, *60*, 7157–7162.
35. Gray, J. J.; Klein, D. H.; Bonnecaze, R. T.; Korgel, B. A. Nonequilibrium Phase Behavior During the Random Sequential Adsorption of Tethered Hard Disks. *Phys. Rev. Lett.* **2000**, *85*, 4430–4433.
36. Lytvyn, P. M.; Strelchuk, V. V.; Kolomys, O. F.; Prokopenko, I. V.; Valakh, M. Y.; Mazur, Y. I.; Wang, Z. M.; Salamo, G. J.; Hanke, M. Two-Dimensional Ordering of (In,Ga)As Quantum Dots in Vertical Multilayers Grown on GaAs(100) and (*n*11). *Appl. Phys. Lett.* **2007**, *91*, 173118.
37. Springholz, G.; Pinczolits, M.; Holy, V.; Zerlauth, S.; Vavra, I.; Bauer, G. Vertical and Lateral Ordering in Self-Organized Quantum Dot Superlattices. *Physica E* **2001**, *9*, 149–163.
38. Deegan, R. D.; Bakajin, O.; Dupont, T. F.; Huber, G.; Nagel, S. R.; Witten, T. A. Capillary Flow as the Cause of Ring Stains from Dried Liquid Drops. *Nature* **1997**, *389*, 827–829.
39. Daniel, S.; Chaudhury, M. K.; Chen, J. C. Fast Drop Movements Resulting From the Phase Change on a Gradient Surface. *Science* **2001**, *291*, 633–636.
40. Maillard, M.; Motte, L.; Ngo, A. T.; Pileni, M. P. Rings and Hexagons Made of Nanocrystals: A Marangoni Effect. *J. Phys. Chem. B* **2000**, *104*, 11871–11877.
41. Smith, D. K.; Goodfellow, B.; Smilgies, D.-M.; Korgel, B. A. Self-Assembled Simple Hexagonal AB2 Binary Nanocrystal Superlattices: SEM, GISAXS, and Defects. *J. Am. Chem. Soc.* **2009**, *131*, 3281–3290.
42. *Landolt-Börnstein, Supplement to IV/18*; Wohlfarth, C., Ed.; Springer: Berlin, Heidelberg, 2009.
43. Yoneda, Y. Anomalous Surface Reflection of X Rays. *Phys. Rev.* **1963**, *131*, 2010.
44. Shah, P. S.; Novick, B. J.; Hwang, H. S.; Lim, K. T.; Carbonell, R. G.; Johnston, K. P.; Korgel, B. A. Kinetics of Nonequilibrium Nanocrystal Monolayer Formation: Deposition From Liquid Carbon Dioxide. *Nano Lett.* **2003**, *3*, 1671–1675.
45. Nolting, W. *Grundkurs Theoretische Physik 6: Statistische Physik*; Springer: Berlin, 2005.
46. Lin, Y.; Skaff, H.; Emrick, T.; Dinsmore, A. D.; Russell, T. P. Nanoparticle Assembly and Transport at Liquid−Liquid Interfaces. *Science* **2003**, *299*, 226–229.
47. Boberl, M.; Kovalenko, M. V.; Gamerith, S.; List, E. J. W.; Heiss, W. Inkjet-Printed Nanocrystal Photodetectors Operating up to 3 μm Wavelengths. *Adv. Mater.* **2007**, *19*, 3574–3578.
48. Tekin, E.; Smith, P. J.; Hoeppener, S.; van den Berg, A. M. J.; Susha, A. S.; Rogach, A. L.; Feldmann, J.; Schubert, U. S. Inkjet Printing of Luminescent CdTe Nanocrystal−Polymer Composites. *Adv. Funct. Mater.* **2007**, *17*, 23–28.
49. Nakashima, H.; Furukawa, K.; Kashimura, Y.; Torimitsu, K. Self-Assembly of Gold Nanorods Induced by Intermolecular Interactions of Surface-Anchored Lipids. *Langmuir* **2008**, *24*, 5654–5658.
50. Bakshi, M. S. A Simple Method of Superlattice Formation: Step-by-Step Evaluation of Crystal Growth of Gold Nanoparticles through Seed-Growth Method. *Langmuir* **2009**, *25*, 12697−12705.
51. Bao, N.; Shen, L.; Padhan, P.; Gupta, A. Self-Assembly and Magnetic Properties of Shape-Controlled Monodisperse $CoFe_2O_4$ Nanocrystals. *Appl. Phys. Lett.* **2008**, *92*, 173101.
52. Song, Q.; John Zhang, Z. Shape Controlled and Associated Magnetic Properties of Spinel Cobalt Ferrite Nanocrystals. *J. Am. Chem. Soc.* **2004**, *126*, 6164–6168.
53. Roth, S. V.; Dohrmann, R.; Dommach, M.; Kuhlmann, M.; Kroger, I.; Gehrke, R.; Walter, H.; Schroer, C.; Lengeler, B.; Muller-Buschbaum, P. Small-Angle Options of the Upgraded Ultrasmall-Angle X-ray Scattering Beamline BW4 at HASYLAB. *Rev. Sci. Instrum.* **2006**, *77*, 085106.
54. Lazzari, R. IsGISAXS: A Program for Grazing-Incidence Small-Angle X-ray Scattering Analysis of Supported Islands. *J. Appl. Crystallogr.* **2002**, *35*, 406–421.
55. Sinha, S. K.; Sirota, E. B.; Garoff, S.; Stanley, H. B. X-ray and Neutron-Scattering from Rough Surfaces. *Phys. Rev. B* **1988**, *38*, 2297–2311.
56. Rauscher, M.; Salditt, T.; Spohn, H. Small-Angle X-ray Scattering under Grazing Incidence: The Cross Section in the Distorted-Wave Born Approximation. *Phys. Rev. B* **1995**, *52*, 16855–16863.